sustainability

Article

Surrogate Model Development for Slope Stability Analysis Using Machine Learning

Xianfeng Li [1,2,*], Mayuko Nishio [3], Kentaro Sugawara [4], Shoji Iwanaga [4] and Pang-jo Chun [1,2]

1 Institute of Engineering Innovation, The University of Tokyo, Tokyo 113-8656, Japan; chun@g.ecc.u-tokyo.ac.jp
2 Department of Civil Engineering, The University of Tokyo, Tokyo 113-8656, Japan
3 Department of Engineering Mechanics and Energy, Faculty of Engineering, Information and Systems, University of Tsukuba, 1-1-1 Tennodai, Tsukuba 305-8573, Japan; nishio@kz.tsukuba.ac.jp
4 Geoscience Research Laboratory, Co., Ltd., 2-3-25 Koraku, Bunkyo City, Tokyo 112-0004, Japan; sugawara@geolab.jp (K.S.); iwanaga@geolab.jp (S.I.)
* Correspondence: li@i-con.t.u-tokyo.ac.jp

Abstract: In many countries, slope failure is a complex natural issue that can result in serious natural hazards, such as landslide dams. It is associated with the challenge of slope stability evaluation, which involves the classification problem of slopes and the regression problem of predicting the factor of safety (FOS) value. This study explored the implementation of machine learning to analyze slope stability using a comprehensive database of 880 homogenous slopes (266 unstable and 614 stable) based on a simulation model developed as a surrogate model. A classification model was developed to categorize slopes into three classes, including S (stable, FOS > 1.2), M (marginally stable, $1.0 \leq$ FOS ≤ 1.2), and U (unstable, FOS < 1.0), and a regression model was used to predict the target FOS value. The results confirmed the efficiency of the developed classification model via testing, achieving an accuracy of 0.9222, with 96.2% accuracy for the U class, 55% for the M class, and 95.2% for the S class. When U and M are in the same class (i.e., the U + M class), the test accuracy is 0.9315, with 93.3% accuracy for the S class and 92.9% accuracy for the U + M class. The low accuracy level for class M led to minor inaccuracies, which can be attributed to a data imbalance. Additionally, the regression model was found to have a high correlation coefficient R-square value of 0.9989 and a low test mean squared error value of 5.03×10^{-4}, which indicates a strong relationship between the FOS values and the selected slope parameters. The significant difference in the elapsed time between the traditional method and the developed surrogate model for slope stability analysis highlights the potential benefits of machine learning.

Keywords: slope stability; factor of safety; machine learning; surrogate model

check for updates

Citation: Li, X.; Nishio, M.; Sugawara, K.; Iwanaga, S.; Chun, P.-j. Surrogate Model Development for Slope Stability Analysis Using Machine Learning. *Sustainability* **2023**, *15*, 10793. https://doi.org/10.3390/su151410793

Academic Editors: Marc A. Rosen, Jiankun Huang, Yunqi Wang, Liqun Lyu and Jun Li

Received: 18 April 2023
Revised: 4 July 2023
Accepted: 5 July 2023
Published: 10 July 2023

1. Introduction

Landslides are common geological hazards that cause significant social and economic damage. These natural hazards are influenced by various factors, including external triggers such as rainfall and earthquakes, as well as internal factors such as slope configuration and soil characteristics [1,2]. It is urgent for engineers and researchers to analyze the stability of slopes to prevent or mitigate the potential risks posed by landslides [3].

Traditionally, slope stability is evaluated by calculating the factor of safety (FOS) and determining an appropriate treatment design. If the FOS is greater than 1.0, the slope is considered stable, whereas if it is less than 1.0, the slope is considered unstable [4]. Common methods for calculating the safety factor in slope stability analyses include the limit equilibrium method (LEM) and numerical calculation methods based on theories of elasticity and plasticity [5,6]. However, the accuracy of the LEM is limited owing to the assumptions about slip surfaces and interslice forces, whereas numerical calculation methods require a precisely fitting constitutive model, which is challenging to achieve [7–9].

The complexity of the interactions among the factors affecting slope stability also makes it challenging to accurately evaluate real slope stability with an FOS.

Machine learning algorithms, such as artificial neural networks (ANNs) [10], support vector machines (SVM) [11], and gradient boosting machines (GBM) [12], have increasingly been used to evaluate slope stability as a nonlinear problem because of their ability to extract valuable information from actual slope case records. These methods evaluate the slope stability based on geotechnical parameters (cohesion and internal friction angle), slope geometry (slope height and slope angle), water conditions (pore water pressure), and dynamic conditions (earthquake effect) and have been proven to be promising in slope stability evaluations. However, even with an FOS > 1.0, the slopes may still fail. According to Mahmoodzadeh et al. [13], slopes with an FOS > 1.2 are considered safe, and the dataset used in previous studies is summarized in their study, which ranged from 10 to 699 cases. Despite the efforts by researchers to collect real on-site data, the dataset is often too small to establish its applicability and repeatability. Therefore, there is a need for surrogate model development [14] in slope stability analysis. The use of machine learning models allows for instantaneous results without the need for numerical simulations, making it an ideal approach.

This study investigates the use of machine learning models to analyze the complex nonlinear relationships in slope stability evaluations, utilizing a comprehensive database of 880 homogenous slopes (266 unstable and 614 stable) generated by FLAC 3D Version 7.0 software (Fast Lagrangian Analysis of Continua in 3 Dimensions, Itasca Company, Minneapolis, MN, USA) instead of traditional real on-site data. A classification model was developed to categorize slopes into three classes: S (stable, FOS > 1.2), M (marginally stable, $1.0 \leq \text{FOS} \leq 1.2$), and U (unstable, FOS < 1.0). Furthermore, a regression model was used to predict the target FOS. This study used virtual slope data to develop the models and evaluate their performance.

2. Dataset

2.1. Modeling: A Simple and Homogeneous Soil Slope

This section models a simple and homogeneous soil slope, with a height of 6 m and an angle of 45°, as shown in Figure 1. The basic slope model had a width of 20 m and a height of 10 m. To maintain the rigid behavior of the model based on the boundary conditions, the slope must be embedded in the bedrock. In the analysis, the unit weight, elastic modulus, and Poisson's ratio of the soil were set at 20 kN/m^3, 14 MPa, and 0.3, respectively. To ensure the validity of the analysis, a range of shear strength properties are utilized, and both numerical simulations using FLAC 3D and analyses using the limit equilibrium method (LEM) were conducted for the parametric study. The FOS results are listed in Table 1.

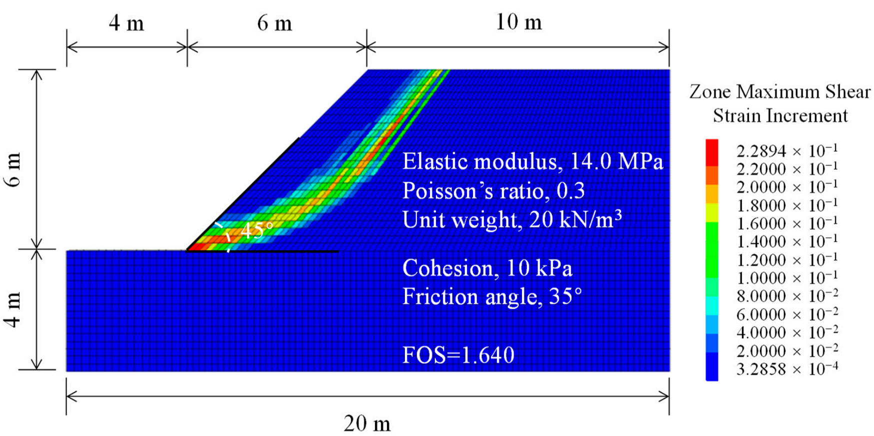

Figure 1. A basic model for a simple and homogeneous soil slope with an FOS of 1.640 using numerical simulation.

Table 1. Factors of safety (FOS) using numerical simulation and LEM.

No.	Cohesion/kPa	Friction Angle/°	FOS *	FOS_LEM [6]	FOS Difference	Relative Error/%
1	2	5	-	0.25	-	-
2	2	15	-	0.50	-	-
3	2	25	-	0.74	-	-
4	2	45	1.15	1.35	0.20	14.81
5	5	5	-	0.41	-	-
6	5	15	-	0.70	-	-
7	5	25	-	0.98	-	-
8	5	35	1.25	1.28	0.03	2.34
9	5	45	1.57	1.65	0.08	4.85
10	10	5	-	0.65	-	-
11	10	15	1.02	0.98	0.04	4.08
12	10	25	1.32	1.30	0.02	1.54
13	10	35	1.64	1.63	0.01	0.61
14	10	45	2.02	2.04	0.02	0.98
15	20	5	1.22	1.06	0.16	15.09
16	20	15	1.59	1.48	0.11	7.43
17	20	25	1.93	1.85	0.08	4.32
18	20	35	2.29	2.24	0.05	2.23
19	20	45	2.73	2.69	0.04	1.49
20	5	0	-	0.20	-	-
21	10	0	-	0.40	-	-
22	20	0	1.00	0.80	0.20	25.00

* '-' means that the FOS value is less than 1.0 without a specified output value.

Therefore, in most cases, the FOS obtained using the numerical simulation is comparable to that obtained using the traditional LEM method under different combinations of soil parameters (i.e., cohesion and internal friction angle). However, there are a few cases in which there is a larger difference in the FOS values between the numerical simulation and the LEM, particularly when the cohesion is 20 kPa and the friction angle is 0°, at which point the error can reach up to 25%. In addition, if the slope is unstable (i.e., FOS is less than 1.0), the numerical simulation analysis does not provide any calculated results. Conversely, if there is no FOS output, the slope is considered unstable.

2.2. An Established Dataset

In this study, several numerical simulations based on FLAC 3D were conducted to model numerous homogenous slopes and obtain their factors of safety (FOS). As aforementioned, all models had a density of 20 kN/m^3, a Young's modulus of 14 MPa, a Poisson's ratio of 0.3, and a tensile strength of 0. Four key parameters were considered to represent the slope characteristics: slope height (H), slope angle (α), cohesion (c), and internal friction angle (φ). Values of 3 m, 6 m, and 9 m were considered for the slope height, and values of 26.57°, 45°, and 63.43° were used for the slope angle. For the soil parameters (shear strength), a range of 2–50 kPa was considered for soil cohesion, and a range of 0–45° was considered for the internal friction angle. This resulted in a dataset consisting of 880 homogenous slopes with FOS values as the output. The generated dataset is shown in Appendix A Table A1. The dataset was then used for the classification model for slopes and the regression model for FOS prediction, which are introduced in Section 3, model development. Note that the dataset used in this study was selected solely by the simple full factorial experiment method, without considering data balance. In addition, the decision to use homogeneous slopes in this study was a deliberate choice made to establish a clear understanding of the neural network's behavior and performance under simplified conditions.

The frequency distribution of the FOS values used in this study is shown in Figure 2, with 266 unstable slopes and 614 stable slopes. To understand the relationship between the

FOS values and other parameters, scatterplots of all key parameters against the FOS are plotted in Figure 3. Additionally, a typical relationship between the FOS and the internal friction angle is shown in Figure 4, with a slope height of 6 m, a slope angle of 45°, and various cohesion values (2–50 kPa). The results indicate that the calculated FOS increases with an increase in both the cohesion and friction angle, which is consistent with previous findings [4]. However, an increase in slope height and slope angle resulted in an initial increase in the FOS, followed by a decrease, which differs from previous research. This discrepancy may be attributed to the range of slope heights and slope angles selected in this study.

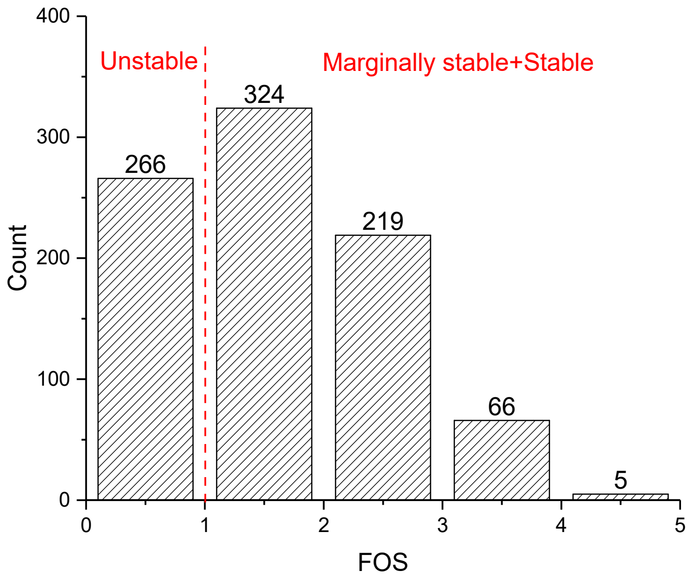

Figure 2. Frequency distribution diagram of the generated FOS database.

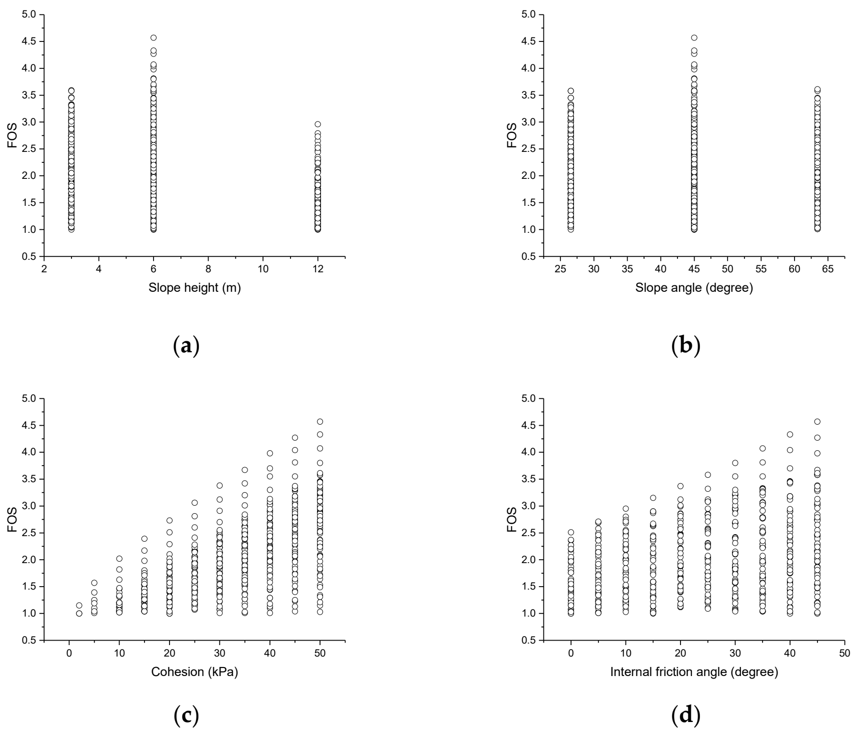

Figure 3. Scatterplots of all input factors: (**a**) slope height, (**b**) slope angle, (**c**) cohesion, and (**d**) internal friction angle with the obtained FOS.

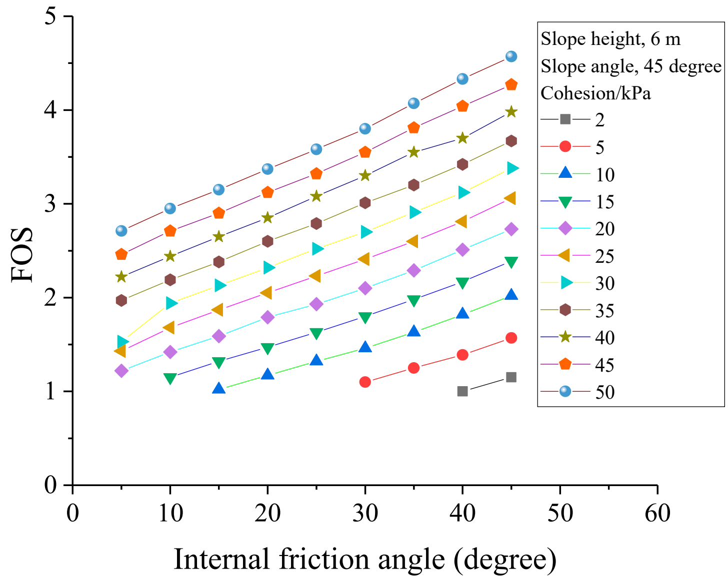

Figure 4. A typical relationship between the FOS and the internal friction angle with slope height of 6 m, slope angle of 45°, and various cohesion values (2–50 kPa).

3. Model Development

Artificial neural networks (ANNs) are machine learning models inspired by the structure and function of the human brain. ANNs are used to model complex relationships between inputs and outputs and can improve their predictions over time [15,16]. In contrast, deep neural networks (DNNs), also known as deep learning models [17], are modifications of ANNs that differ primarily in the number of layers they contain [18]. While ANNs have a single layer of input neurons connected to a single layer of output neurons, DNNs consist of multiple layers of neurons, with each layer feeding into the next. The increased complexity of DNNs enables them to learn and identify complex features and patterns in data that may not be apparent in simpler models such as ANNs.

DNNs have a wide range of applications in civil engineering, including crack detection in concrete [19] and asphalt pavement [20], bridge damage identification [21,22], and the automatic recognition of soil desiccation cracks [23]. Overall, the greater complexity and improved feature recognition capabilities of DNNs make them powerful tools for a variety of machine learning tasks (e.g., classification and regression), particularly those involving large and complex datasets. Additionally, the use of a surrogate model with machine learning can help reduce the computation time and cost.

3.1. A Deep Neural Network Model for Slope Classification

A deep neural network for classification is a machine learning tool used to categorize input data into different classes [24]. This model facilitates data collection, network creation and training, and performance evaluation using cross-entropy and confusion matrices. A trained, feedforward, and fully connected DNN model designed for slope classification is shown in Figure 5. This network consisted of nine fully connected hidden layers, with each subsequent layer receiving input from the previous layer. The first hidden layer was connected to the network input. Each layer adjusts the input via a weight matrix and the addition of a bias vector, and the final layer, followed by the application of a softmax activation function, produces the network output in the form of classification labels. The hidden layer has a neuron size of {8 16 16 32 16 32 16 16 8}, determined by trial and error, which ensures excellent performance. The output has three classes, i.e., S (stable, FOS > 1.2), M (marginally stable, 1.0 ≤ FOS ≤ 1.2), and U (unstable, FOS < 1.0). When U and M are in the same class, the output has two classes: S and U + M. The process of building a deep neural network for classification typically includes the following steps:

(a) Data preprocessing: The first step is to prepare the input data and target labels used to train the network. This typically involves dividing the data into training and test sets.
(b) Network construction and training: The next step is to train the network using the training data. A DNN model is trained on the input data, which requires specifying the input data, target labels, and the type of network to be trained.
(c) Prediction: Once the network is trained, the model can be used to predict the test set.
(d) Performance evaluation: The performance of the network can be evaluated using a confusion matrix.

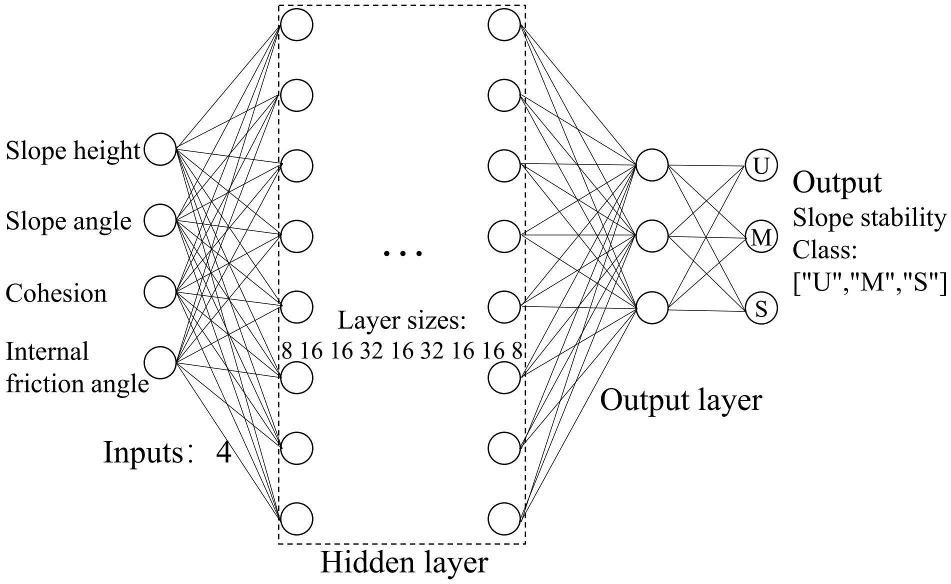

Figure 5. A deep neural network model for slope classification.

3.2. A Deep Neural Network Model for the Factor of Safety Regression

A DNN for regression is a machine learning technique that utilizes neural networks to predict numerical values from input data [17,25]. Furthermore, it involves training a network using input data and their corresponding target values and generating predicted values for new input data. In this study, a feedforward DNN model was designed for FOS regression. The network architecture was similar to that of the DNN model used for classification, with the main difference being the output value. In the regression network, the predicted target values (FOS) were generated by the final fully connected layer. Using trial and error, the DNN model for regression consisted of 11 layers with neuron sizes of {8 16 16 32 32 64 32 32 16 16 8}, as illustrated in Figure 6. The procedure for a regression DNN typically involves the following steps:

(a) Data preprocessing: The dataset is divided into training and test sets, and necessary preprocessing steps such as feature normalization and the handling of missing values are performed.
(b) Network construction and training: A DNN consisting of input, hidden, and output layers is constructed, with the architecture of the network determined by factors such as the number of hidden layers and nodes. The network is trained using a training set.
(c) Prediction: The trained model is utilized to generate predicted values for new input data.
(d) Performance evaluation: The performance of the model was evaluated using metrics such as the mean squared error (MSE) and correlation coefficient R-square value.

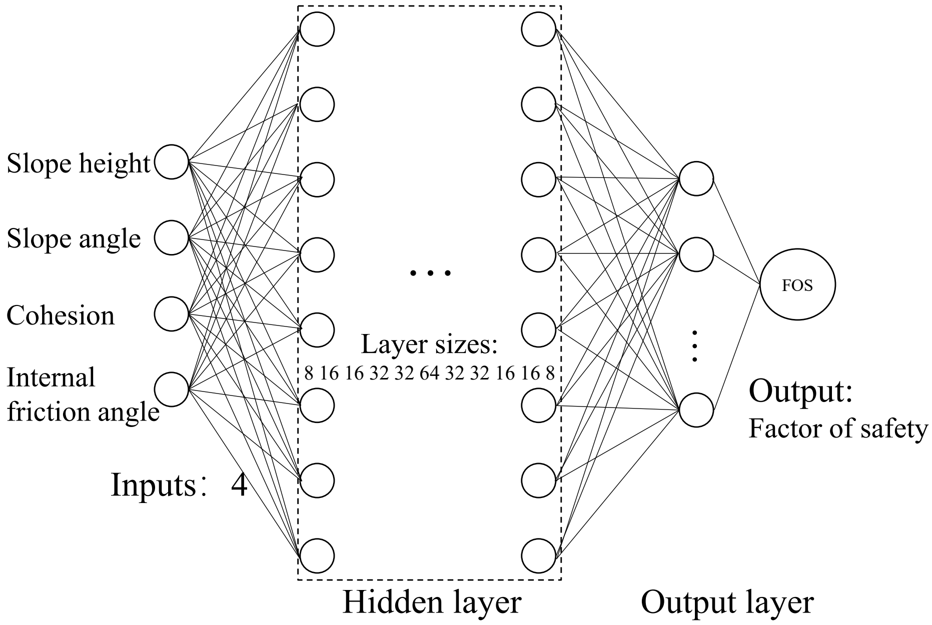

Figure 6. A deep neural network model for regression.

4. Results and Discussion

4.1. Slope Classification

In this study, 70% of the generated dataset was used to train the machine learning classification model, and the remaining 30% was used for testing. To eliminate subjectivity in data selection, both the training and test datasets were randomly selected. The rectified linear unit (ReLU) function was used as the action function for the classification model. Table 2 lists the training error and accuracy for three classes (S, M, and U) and two classes (S and U + M). For three classes, the training accuracy was 0.9919 with a training error of 0.0081, whereas for two classes, the training accuracy was 0.9692 with a training error of 0.0308. Both had high accuracies (>0.9000).

Table 2. Error and accuracy of training, cross-validation training, and test sets.

Output		Training	Cross-Validation Training	Test
Three classes	Error	0.0081	0.1104	0.0778
	Accuracy	0.9919	0.8896	0.9222
Two classes	Error	0.0308	0.0908	0.0685
	Accuracy	0.9692	0.9092	0.9315

For the three classes, using the model to predict the test set, the test accuracy of the model was approximately 0.9222 with a test error of 0.0778. According to the confusion matrix in Figure 7a, the test accuracy for the U (unstable) and S (stable) classes was above 95%, whereas that for the M (marginally stable) class was approximately 55%, owing to a data imbalance. Therefore, class M had relatively fewer cases than the other two classes. For example, referring to the dataset in Appendix A Table A1, the M class has just 76 cases because the range of the FOS is relatively small, from 1.0 to 1.2, while the U class has 266 cases, and the S class has 538 cases. Thus, the generated class M was significantly smaller than the other two classes. However, class M is marginally stable; thus, it is probably stable and unstable. Such an M-class slope is also extremely dangerous and requires more attention to avoid slope failures. This classification model was developed to classify slopes into three classes, including S (stable), M (marginally stable), and U (unstable), with a higher test accuracy of over 90%.

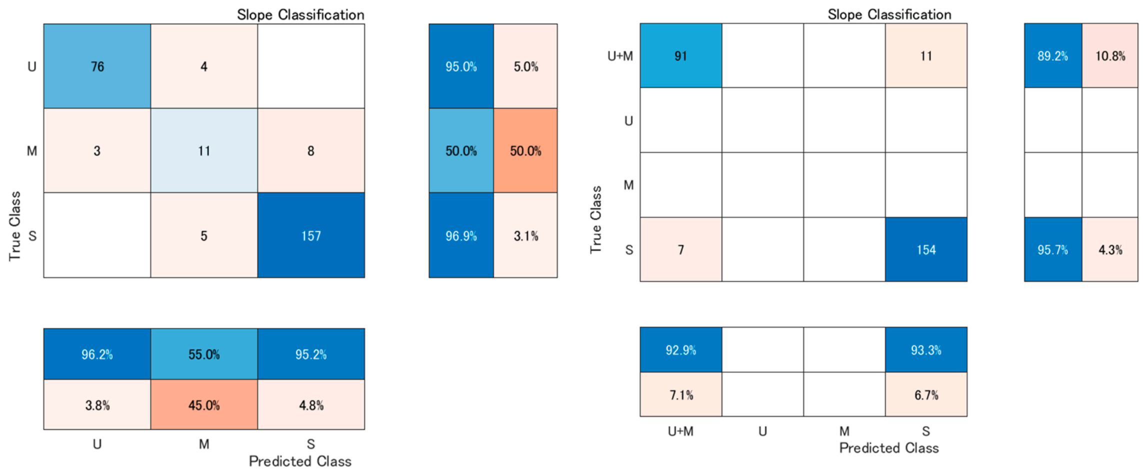

(**a**) (**b**)

Figure 7. Confusion matrix for the test set: (**a**) three classes and (**b**) two classes.

Similarly, when U and M are in the same class, another classification model was developed to categorize the slopes into two classes: S (stable, FOS > 1.2) and U + M (unstable, FOS < 1.2). Using this training model to predict the test set, the test accuracy was approximately 0.9315, which was slightly higher than the accuracy of the three-class model, and the test error was 0.0685. Figure 7b presents the confusion matrix for the test set, showing that the test accuracy for the S (stable) class was 93.3%, and the test accuracy for the U + M class was approximately 92.9%, both exceeding 90.0%. Thus, this classification model was also developed to classify slopes into two classes, S (stable) and U + M (unstable), with a higher test accuracy of over 90%. Regardless of the class, the machine learning model had a high accuracy of more than 90%. If the dataset is sufficient, the three classes are considered superior.

However, the cross-validation misclassification error provides an estimate of how well a model performs on the new data. In this study, a 10-fold cross-validation was conducted, and the findings are presented in Table 2. Therefore, for the three classes, the cross-validation training error of 0.1104 was higher than the training error of 0.0081, which was much closer to the test error of 0.0778. In addition, the cross-validation accuracy of 0.8896 was lower than the training accuracy of 0.9919, which was much closer to the test accuracy of 0.9222. Therefore, relying solely on the misclassification error of the training data underestimates the misclassification rate of the new data. Consequently, the cross-validation error provided a more accurate estimate of the performance of the model on the new data than the training error. Similar findings were also observed for both classes.

4.2. Slope FOS Prediction

In this study, 80% of the generated dataset was allocated to training, and the training and test sets were randomly selected. The ReLU function was selected as the activation function for the regression DNN model, with linear activation used as the output layer. Thus, 704 data points were used to construct the machine learning regression model with four input parameters (slope height, slope angle, cohesion, and internal friction angle) and one output target value of the FOS. Figure 8 displays the training loss curve with iterations, and Figure 9 depicts the relationship between the "true" FOS and the predicted FOS for the test set on slopes based on the regression model. The mean squared error (MSE) for the test set was approximately 5.03×10^{-4}, and the correlation coefficient R-square for the regression model was 0.9989, indicating a strong linear relationship between the predicted FOS value and the true FOS obtained by numerical simulation. This means that this regression model can be used to predict FOS accurately. Thus, the regression model accurately predicted the FOS value and effectively modeled the relationship between the FOS values and the selected slope parameters.

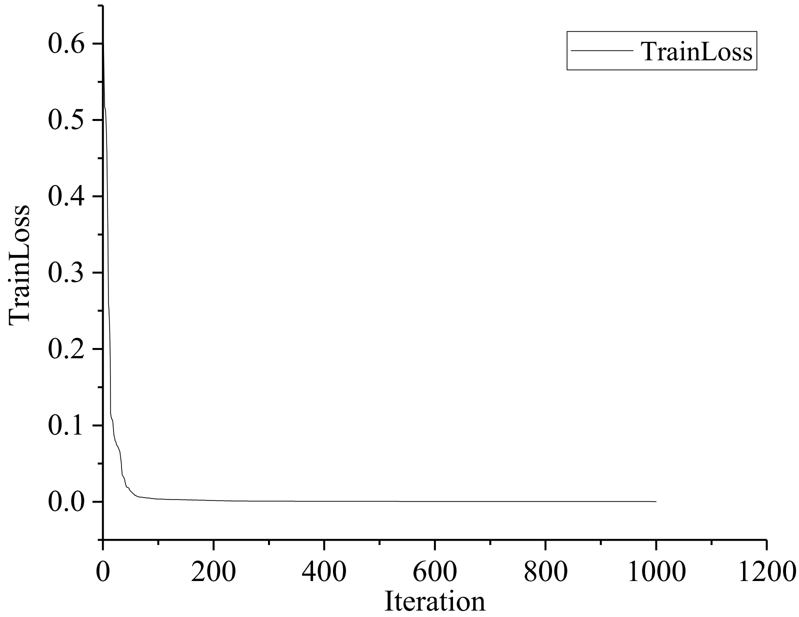

Figure 8. Training loss curve.

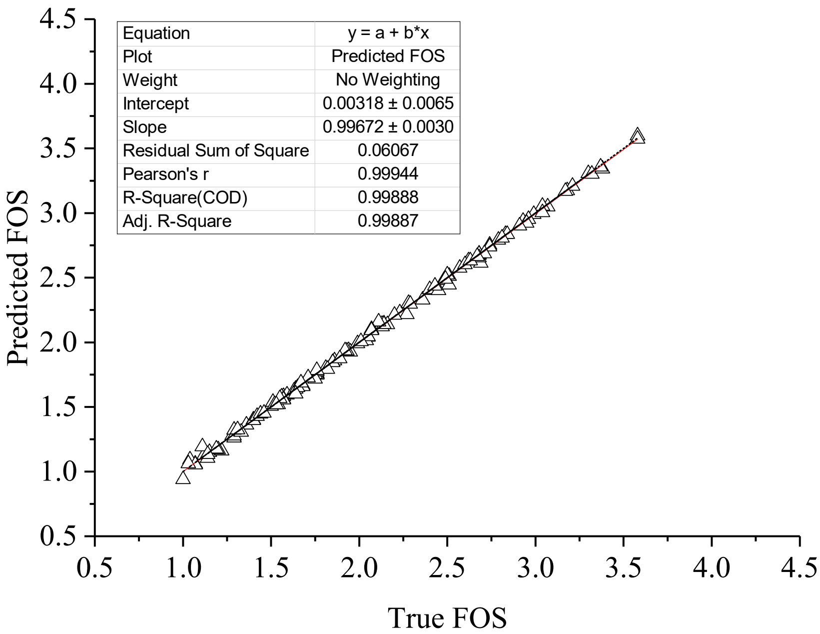

Figure 9. The relationship between the predicted FOS and the "true" FOS using numerical simulation based on the test set.

Actually, the FOS provides a quantitative assessment of slope stability. Calculating the FOS is essential in slope stability analysis to evaluate safety, optimize design, manage risks, support decision making, and comply with regulatory requirements. The proper assessment and control of the FOS are essential for ensuring the long-term stability and reliability of slopes. Therefore, the regression model used to predict the factor of safety (FOS) holds significant meaning for engineering practices.

4.3. Time Consumption

Table 3 presents a comparison of the times consumed by the various calculation methods for slope stability analysis. The traditional method, which uses FLAC 3D to determine the FOS, requires approximately 125 s for a typical case, as shown in Figure 1. In contrast, using the machine learning model for classification, the elapsed times for the training and test set classification of the 880 datasets for the three classes were only 1.549320 s and 0.001513 s, respectively. Similarly, for regression, the elapsed times for the training and test set regressions of the 880 datasets were only 0.045756 s and 0.003117 s, respectively. These results show that a surrogate model based on machine learning can be utilized to predict the FOS values in real time. The significant difference in the elapsed time between the traditional method and the developed surrogate model for slope stability analysis highlights the potential benefits of machine learning. By allowing quick and accurate predictions of the FOS, decision makers can take prompt action to prevent and mitigate hazards, thereby reducing the risk of accidents and damage. Consequently, such a surrogate model using machine learning models can complement traditional computational methods, accelerate the FOS prediction process, and contribute to the development of effective and efficient risk management strategies.

Table 3. Time consumption of various calculation methods for slope stability analysis.

Methods	**Numerical Simulation**	**Classification (Three Classes)**		**Regression**	
Set	**-**	**Training**	**Test**	**Training**	**Test**
Case No.	1	616 (70%)	264 (30%)	704 (80%)	176 (20%)
Time/s	125	1.549320	0.001513	0.045756	0.003117

4.4. Discussion

Using the traditional limit equilibrium method (LEM), the factor of safety is defined by the following equation [26]:

$$FOS = \frac{shear\ strength\ of\ soil}{shear\ stress\ required\ for\ equilibrium}, \tag{1}$$

It can also be expressed as follows:

$$FOS = \frac{\tau_{fi}}{\tau_i} = \frac{c + \sigma_i tan\varphi}{\tau_i}, \tag{2}$$

where τ_i and σ_i are the shear stress and normal stress at the *i*-th slice of the slip surface, respectively, and c and φ are the cohesion and internal friction angle, respectively. The critical slip surface corresponds to the surface that yields the lowest factor of safety (FOS), with this minimal value representing the true FOS.

According to the defined FOS by LEM, the cohesion and internal friction angle play crucial roles as parameters. As the surrogate model can predict the FOS, a comparison between the typical FOS calculations (based on Table 1; data with the FOS less than 1.0 have been removed) obtained from the traditional LEM method and the surrogate model is listed in Table 4. The results indicate that the developed surrogate model can accurately predict the FOS value. When the FOS obtained from the LEM method exceeds 1.0, the relative error is mostly below 10%, except for Case No. 4, which reaches approximately 15%. It is believed that enhancing the accuracy of the surrogate model would require a larger and more diverse dataset. The traditional method primarily focuses on the cohesion and friction angle, whereas the surrogate model incorporates two additional factors related to slope shape: slope height and slope angle. Although further improvements are necessary to enhance the accuracy of the surrogate model, Section 4.3 demonstrates the effectiveness of this approach.

Table 4. Typical factors of safety (FOS) using LEM and the developed surrogate model.

No.	Cohesion/kPa	Friction Angle/°	FOS_LEM [6]	FOS by Surrogate Model	The Difference	Relative Error/%
4	2	45	1.35	1.16	−0.19	−14.37
8	5	35	1.28	1.24	−0.04	−3.41
9	5	45	1.65	1.54	−0.11	−6.72
12	10	25	1.30	1.33	0.03	1.97
13	10	35	1.63	1.63	0.00	0.04
14	10	45	2.04	2.02	−0.02	−1.05
15	20	5	1.06	1.16	0.10	9.58
16	20	15	1.48	1.60	0.12	8.11
17	20	25	1.85	1.93	0.08	4.56
18	20	35	2.24	2.29	0.05	2.40
19	20	45	2.69	2.75	0.06	2.21

By incorporating the findings of the surrogate model into traditional studies, researchers can enhance the efficiency of slope stability assessments. This integration allows for a more comprehensive analysis and a deeper understanding of slope behavior, ultimately leading to improved engineering practices and decision making in geotechnical engineering.

The surrogate model can be used to calibrate and validate traditional LEM parameters. By comparing the FOS predictions of the surrogate model with the results obtained from the LEM, researchers may assess the accuracy and reliability of the traditional method. This helps in fine-tuning the LEM parameters and improving its predictive capabilities. Additionally, researchers can systematically vary the input parameters within a range and observe the corresponding changes in the FOS predicted by the surrogate model. This analysis provides insights into the relative importance and influence of different factors on slope stability, aiding researchers in identifying critical parameters and optimizing their analyses.

4.5. Contributions, Limitations, and Further Research

The main strength of this work lies in the proposal of a surrogate model using machine learning to evaluate slope stability and compare the FOS value with the traditional LEM method. This study contributes to slope analysis in the following ways: (a) expanding classifications: the concept of a marginally stable class for slopes is introduced, which challenges the traditional binary classification of stable and unstable slopes; (b) surrogate modeling: the study showcases the potential of surrogate models in slope stability analysis, offering a cost-effective and time-efficient alternative to traditional methods.

Thus, when conducting a slope stability analysis, the classification model can be used first. Table 5 summarizes the countermeasures based on the slope classification. In cases in which the result falls into class U, prompt treatment should be considered, such as modifying the slope shape (slope height and slope angle) or increasing the strength of the soil (cohesion and friction angle) using methods like water drainage. Additionally, the regression model can also be used to obtain the FOS for slope analysis if it exceeds 1.0. For slopes classified as class M, real-time monitoring and early warning are necessary to prevent sudden slope failure. When the slope is classified as class S, regular monitoring and maintenance can be implemented based on the FOS values. A higher FOS indicates a greater safety margin for the slope. The proposed countermeasures can be applied to the slope to prevent or mitigate the potential risks posed by landslides.

However, this work has several limitations that need to be acknowledged. Firstly, there is a lack of empirical validation for the surrogate model, specifically regarding its ability to accurately predict unstable slopes leading to landslide events. As a result, the utilization of this model for decision making purposes requires further clarification and study. Another limitation of the current study is its focus on homogeneous slopes with constant Mohr–

Coulomb shear strength parameters. Future studies should aim to incorporate more realistic conditions that closely resemble actual field sites. For instance, researchers can consider incorporating complex soil and/or rock layers, as well as variations in other factors such as pore water pressure, rainfall, and seismic events. In doing so, the applicability and validity of the findings in practical scenarios can be enhanced. A final limitation worth noting is the issue of data imbalance, which requires greater attention.

Table 5. Proposed countermeasures based on the surrogate model.

Slope Classification	FOS	Countermeasures
U	<1.0	Prompt treatment
M	$1.0 \leq$ FOS ≤ 1.2	Monitoring and early warning
S	>1.2	Regular monitoring and maintenance

In future studies, it is recommended to utilize newer and more diverse datasets with various input parameters to predict the factor of safety (FOS) in different slopes. This approach would help identify the most accurate algorithms and determine the most effective parameters that influence slope stability. In conclusion, while this work presents a valuable contribution to slope stability analysis, it is important to address the aforementioned limitations in future studies to further refine the models and enhance their applicability and reliability.

5. Conclusions

This study investigated the application of a surrogate model using machine learning to evaluate slope stability by capturing the intricate nonlinear and multidimensional relationships between the parameters. The slope analysis problem is divided into two parts: the classification of slopes into stable, marginally stable, and unstable classes and regression to predict the factor of safety (FOS) value. This study utilized a comprehensive database of 880 homogeneous slopes generated by the FLAC 3D Version 7.0 software for surrogate model development. The classification model was efficient, achieving a test accuracy of 0.9222, with a class accuracy of 96.2% for the U class (unstable), 55% for the M class (marginally stable), and 95.2% for the S class (stable). When U and M are in the same class (i.e., the U + M class), the test accuracy is 0.9315, with 93.3% accuracy for the S class and 92.9% accuracy for the U + M class. The regression model demonstrated a high correlation coefficient R-square value of 0.9989 and a low test MSE value of 5.03×10^{-4}, indicating a strong relationship between the FOS values and the selected slope parameters. However, the generated dataset may not be representative of all the actual site conditions, and more complex geological conditions and other input factors must be considered. Moreover, such a surrogate model can complement traditional computational methods and accelerate the prediction of the FOS in slope stability analysis. This capability enables decision makers to promptly take the necessary actions to prevent and mitigate potential hazards, thus contributing to the development of effective and efficient risk management strategies. Incorporating surrogate models into slope stability problems can effectively achieve long-term sustainability while minimizing risks and preserving natural resources.

Author Contributions: Conceptualization, X.L., M.N. and P.-j.C.; methodology, X.L.; software, K.S., S.I. and X.L.; validation, X.L., M.N. and P.-j.C.; formal analysis, X.L.; writing—original draft preparation, X.L.; writing—review and editing, M.N. and P.-j.C.; supervision, M.N. and P.-j.C.; funding acquisition, M.N. and P.-j.C. All authors have read and agreed to the published version of the manuscript.

Funding: This research was funded by JST (Moonshot Research and Development) (grant number JPMJMS2032).

Institutional Review Board Statement: Not applicable.

Informed Consent Statement: Not applicable.

Data Availability Statement: The data presented in this study are available upon reasonable request from the corresponding author.

Acknowledgments: The authors would like to extend their sincere gratitude to the reviewers for their invaluable contributions and insightful feedback, which have greatly improved the quality of this research.

Conflicts of Interest: The authors declare no conflict of interest.

Appendix A

Table A1. Dataset used in this study.

Case No.	Slope Height/m	Slope Angle/°	Cohesion/kPa	Friction Angle/°	FOS	Labels
1	3	26.57	2	5	-	U
2	3	26.57	2	10	-	U
3	3	26.57	2	15	-	U
4	3	26.57	2	20	-	U
5	3	26.57	2	25	-	U
6	3	26.57	2	30	-	U
7	3	26.57	2	35	-	U
8	3	26.57	2	40	-	U
9	3	26.57	2	45	-	U
10	3	26.57	5	5	-	U
11	3	26.57	5	10	-	U
12	3	26.57	5	15	-	U
13	3	26.57	5	20	-	U
14	3	26.57	5	25	-	U
15	3	26.57	5	30	-	U
16	3	26.57	5	35	-	U
17	3	26.57	5	40	-	U
18	3	26.57	5	45	-	U
19	3	26.57	10	5	-	U
20	3	26.57	10	10	-	U
21	3	26.57	10	15	-	U
22	3	26.57	10	20	-	U
23	3	26.57	10	25	-	U
24	3	26.57	10	30	-	U
25	3	26.57	10	35	1.04	M
26	3	26.57	10	40	1.12	M
27	3	26.57	10	45	1.2	M
28	3	26.57	15	5	-	U
29	3	26.57	15	10	-	U
30	3	26.57	15	15	1.04	M
31	3	26.57	15	20	1.12	M
32	3	26.57	15	25	1.2	M

Table A1. *Cont.*

Case No.	Slope Height/m	Slope Angle/°	Cohesion/kPa	Friction Angle/°	FOS	Labels
33	3	26.57	15	30	1.28	S
34	3	26.57	15	35	1.36	S
35	3	26.57	15	40	1.46	S
36	3	26.57	15	45	1.54	S
37	3	26.57	20	5	1.14	M
38	3	26.57	20	10	1.23	S
39	3	26.57	20	15	1.31	S
40	3	26.57	20	20	1.4	S
41	3	26.57	20	25	1.49	S
42	3	26.57	20	30	1.57	S
43	3	26.57	20	35	1.67	S
44	3	26.57	20	40	1.76	S
45	3	26.57	20	45	1.86	S
46	3	26.57	25	5	1.4	S
47	3	26.57	25	10	1.49	S
48	3	26.57	25	15	1.58	S
49	3	26.57	25	20	1.68	S
50	3	26.57	25	25	1.76	S
51	3	26.57	25	30	1.85	S
52	3	26.57	25	35	1.95	S
53	3	26.57	25	40	2.05	S
54	3	26.57	25	45	2.17	S
55	3	26.57	30	5	1.67	S
56	3	26.57	30	10	1.76	S
57	3	26.57	30	15	1.85	S
58	3	26.57	30	20	1.93	S
59	3	26.57	30	25	2.04	S
60	3	26.57	30	30	2.13	S
61	3	26.57	30	35	2.23	S
62	3	26.57	30	40	2.34	S
63	3	26.57	30	45	2.46	S
64	3	26.57	35	5	1.91	S
65	3	26.57	35	10	2.02	S
66	3	26.57	35	15	2.12	S
67	3	26.57	35	20	2.21	S
68	3	26.57	35	25	2.3	S
69	3	26.57	35	30	2.4	S
70	3	26.57	35	35	2.51	S
71	3	26.57	35	40	2.62	S
72	3	26.57	35	45	2.74	S

Table A1. *Cont.*

Case No.	Slope Height/m	Slope Angle/°	Cohesion/kPa	Friction Angle/°	FOS	Labels
73	3	26.57	40	5	2.16	S
74	3	26.57	40	10	2.29	S
75	3	26.57	40	15	2.38	S
76	3	26.57	40	20	2.48	S
77	3	26.57	40	25	2.57	S
78	3	26.57	40	30	2.68	S
79	3	26.57	40	35	2.79	S
80	3	26.57	40	40	2.9	S
81	3	26.57	40	45	3.02	S
82	3	26.57	45	5	2.41	S
83	3	26.57	45	10	2.55	S
84	3	26.57	45	15	2.64	S
85	3	26.57	45	20	2.74	S
86	3	26.57	45	25	2.83	S
87	3	26.57	45	30	2.93	S
88	3	26.57	45	35	3.07	S
89	3	26.57	45	40	3.18	S
90	3	26.57	45	45	3.3	S
91	3	26.57	50	5	2.69	S
92	3	26.57	50	10	2.8	S
93	3	26.57	50	15	2.9	S
94	3	26.57	50	20	3	S
95	3	26.57	50	25	3.1	S
96	3	26.57	50	30	3.2	S
97	3	26.57	50	35	3.33	S
98	3	26.57	50	40	3.45	S
99	3	26.57	50	45	3.58	S
100	3	26.57	2	0	-	U
101	3	26.57	5	0	-	U
102	3	26.57	10	0	-	U
103	3	26.57	15	0	-	U
104	3	26.57	20	0	1	M
105	3	26.57	25	0	1.25	S
106	3	26.57	30	0	1.5	S
107	3	26.57	35	0	1.76	S
108	3	26.57	40	0	2.02	S
109	3	26.57	45	0	2.27	S
110	3	26.57	50	0	2.51	S
111	3	45	2	5	-	U
112	3	45	2	10	-	U

Table A1. *Cont.*

Case No.	Slope Height/m	Slope Angle/°	Cohesion/kPa	Friction Angle/°	FOS	Labels
113	3	45	2	15	-	U
114	3	45	2	20	-	U
115	3	45	2	25	-	U
116	3	45	2	30	-	U
117	3	45	2	35	-	U
118	3	45	2	40	-	U
119	3	45	2	45	-	U
120	3	45	5	5	-	U
121	3	45	5	10	-	U
122	3	45	5	15	-	U
123	3	45	5	20	-	U
124	3	45	5	25	-	U
125	3	45	5	30	-	U
126	3	45	5	35	-	U
127	3	45	5	40	-	U
128	3	45	5	45	-	U
129	3	45	10	5	-	U
130	3	45	10	10	-	U
131	3	45	10	15	-	U
132	3	45	10	20	-	U
133	3	45	10	25	-	U
134	3	45	10	30	-	U
135	3	45	10	35	1.04	M
136	3	45	10	40	1.12	M
137	3	45	10	45	1.2	M
138	3	45	15	5	-	U
139	3	45	15	10	-	U
140	3	45	15	15	1.04	M
141	3	45	15	20	1.13	M
142	3	45	15	25	1.21	S
143	3	45	15	30	1.28	S
144	3	45	15	35	1.36	S
145	3	45	15	40	1.44	S
146	3	45	15	45	1.54	S
147	3	45	20	5	1.13	M
148	3	45	20	10	1.23	S
149	3	45	20	15	1.31	S
150	3	45	20	20	1.41	S
151	3	45	20	25	1.49	S
152	3	45	20	30	1.57	S

Table A1. *Cont.*

Case No.	Slope Height/m	Slope Angle/°	Cohesion/kPa	Friction Angle/°	FOS	Labels
153	3	45	20	35	1.67	S
154	3	45	20	40	1.76	S
155	3	45	20	45	1.87	S
156	3	45	25	5	1.38	S
157	3	45	25	10	1.49	S
158	3	45	25	15	1.59	S
159	3	45	25	20	1.68	S
160	3	45	25	25	1.76	S
161	3	45	25	30	1.85	S
162	3	45	25	35	1.95	S
163	3	45	25	40	2.06	S
164	3	45	25	45	2.16	S
165	3	45	30	5	1.63	S
166	3	45	30	10	1.75	S
167	3	45	30	15	1.85	S
168	3	45	30	20	1.94	S
169	3	45	30	25	2.04	S
170	3	45	30	30	2.14	S
171	3	45	30	35	2.23	S
172	3	45	30	40	2.34	S
173	3	45	30	45	2.46	S
174	3	45	35	5	1.85	S
175	3	45	35	10	2.01	S
176	3	45	35	15	2.12	S
177	3	45	35	20	2.2	S
178	3	45	35	25	2.31	S
179	3	45	35	30	2.42	S
180	3	45	35	35	2.5	S
181	3	45	35	40	2.61	S
182	3	45	35	45	2.74	S
183	3	45	40	5	2.12	S
184	3	45	40	10	2.25	S
185	3	45	40	15	2.39	S
186	3	45	40	20	2.47	S
187	3	45	40	25	2.58	S
188	3	45	40	30	2.69	S
189	3	45	40	35	2.77	S
190	3	45	40	40	2.91	S
191	3	45	40	45	3.02	S
192	3	45	45	5	2.36	S

Table A1. *Cont.*

Case No.	Slope Height/m	Slope Angle/°	Cohesion/kPa	Friction Angle/°	FOS	Labels
193	3	45	45	10	2.5	S
194	3	45	45	15	2.63	S
195	3	45	45	20	2.74	S
196	3	45	45	25	2.85	S
197	3	45	45	30	2.94	S
198	3	45	45	35	3.04	S
199	3	45	45	40	3.18	S
200	3	45	45	45	3.32	S
201	3	45	50	5	2.58	S
202	3	45	50	10	2.74	S
203	3	45	50	15	2.88	S
204	3	45	50	20	2.99	S
205	3	45	50	25	3.1	S
206	3	45	50	30	3.21	S
207	3	45	50	35	3.32	S
208	3	45	50	40	3.46	S
209	3	45	50	45	3.59	S
210	3	45	2	0	-	U
211	3	45	5	0	-	U
212	3	45	10	0	-	U
213	3	45	15	0	-	U
214	3	45	20	0	-	U
215	3	45	25	0	1.17	M
216	3	45	30	0	1.4	S
217	3	45	35	0	1.64	S
218	3	45	40	0	1.87	S
219	3	45	45	0	2.13	S
220	3	45	50	0	2.36	S
221	3	63.43	2	5	-	U
222	3	63.43	2	10	-	U
223	3	63.43	2	15	-	U
224	3	63.43	2	20	-	U
225	3	63.43	2	25	-	U
226	3	63.43	2	30	-	U
227	3	63.43	2	35	-	U
228	3	63.43	2	40	-	U
229	3	63.43	2	45	-	U
230	3	63.43	5	5	-	U
231	3	63.43	5	10	-	U
232	3	63.43	5	15	-	U

Table A1. *Cont.*

Case No.	Slope Height/m	Slope Angle/°	Cohesion/kPa	Friction Angle/°	FOS	Labels
233	3	63.43	5	20	-	U
234	3	63.43	5	25	-	U
235	3	63.43	5	30	-	U
236	3	63.43	5	35	-	U
237	3	63.43	5	40	-	U
238	3	63.43	5	45	-	U
239	3	63.43	10	5	-	U
240	3	63.43	10	10	-	U
241	3	63.43	10	15	-	U
242	3	63.43	10	20	-	U
243	3	63.43	10	25	-	U
244	3	63.43	10	30	-	U
245	3	63.43	10	35	1.04	M
246	3	63.43	10	40	1.12	M
247	3	63.43	10	45	1.2	M
248	3	63.43	15	5	-	U
249	3	63.43	15	10	-	U
250	3	63.43	15	15	1.05	M
251	3	63.43	15	20	1.12	M
252	3	63.43	15	25	1.21	S
253	3	63.43	15	30	1.29	S
254	3	63.43	15	35	1.36	S
255	3	63.43	15	40	1.45	S
256	3	63.43	15	45	1.53	S
257	3	63.43	20	5	1.12	M
258	3	63.43	20	10	1.23	S
259	3	63.43	20	15	1.31	S
260	3	63.43	20	20	1.4	S
261	3	63.43	20	25	1.48	S
262	3	63.43	20	30	1.57	S
263	3	63.43	20	35	1.67	S
264	3	63.43	20	40	1.75	S
265	3	63.43	20	45	1.86	S
266	3	63.43	25	5	1.34	S
267	3	63.43	25	10	1.5	S
268	3	63.43	25	15	1.59	S
269	3	63.43	25	20	1.68	S
270	3	63.43	25	25	1.75	S
271	3	63.43	25	30	1.85	S
272	3	63.43	25	35	1.94	S

Table A1. *Cont.*

Case No.	Slope Height/m	Slope Angle/°	Cohesion/kPa	Friction Angle/°	FOS	Labels
273	3	63.43	25	40	2.05	S
274	3	63.43	25	45	2.16	S
275	3	63.43	30	5	1.59	S
276	3	63.43	30	10	1.74	S
277	3	63.43	30	15	1.85	S
278	3	63.43	30	20	1.95	S
279	3	63.43	30	25	2.04	S
280	3	63.43	30	30	2.13	S
281	3	63.43	30	35	2.23	S
282	3	63.43	30	40	2.32	S
283	3	63.43	30	45	2.44	S
284	3	63.43	35	5	1.8	S
285	3	63.43	35	10	1.99	S
286	3	63.43	35	15	2.1	S
287	3	63.43	35	20	2.2	S
288	3	63.43	35	25	2.3	S
289	3	63.43	35	30	2.4	S
290	3	63.43	35	35	2.51	S
291	3	63.43	35	40	2.63	S
292	3	63.43	35	45	2.75	S
293	3	63.43	40	5	2.05	S
294	3	63.43	40	10	2.22	S
295	3	63.43	40	15	2.35	S
296	3	63.43	40	20	2.46	S
297	3	63.43	40	25	2.57	S
298	3	63.43	40	30	2.68	S
299	3	63.43	40	35	2.79	S
300	3	63.43	40	40	2.9	S
301	3	63.43	40	45	3.04	S
302	3	63.43	45	5	2.27	S
303	3	63.43	45	10	2.46	S
304	3	63.43	45	15	2.63	S
305	3	63.43	45	20	2.74	S
306	3	63.43	45	25	2.85	S
307	3	63.43	45	30	2.96	S
308	3	63.43	45	35	3.06	S
309	3	63.43	45	40	3.17	S
310	3	63.43	45	45	3.28	S
311	3	63.43	50	5	2.49	S
312	3	63.43	50	10	2.68	S

Table A1. *Cont.*

Case No.	Slope Height/m	Slope Angle/°	Cohesion/kPa	Friction Angle/°	FOS	Labels
313	3	63.43	50	15	2.87	S
314	3	63.43	50	20	3.01	S
315	3	63.43	50	25	3.12	S
316	3	63.43	50	30	3.23	S
317	3	63.43	50	35	3.31	S
318	3	63.43	50	40	3.45	S
319	3	63.43	50	45	3.58	S
320	3	63.43	2	0	-	U
321	3	63.43	5	0	-	U
322	3	63.43	10	0	-	U
323	3	63.43	15	0	-	U
324	3	63.43	20	0	-	U
325	3	63.43	25	0	1.15	M
326	3	63.43	30	0	1.36	S
327	3	63.43	35	0	1.56	S
328	3	63.43	40	0	1.81	S
329	3	63.43	45	0	2.05	S
330	3	63.43	50	0	2.27	S
331	6	26.57	2	5	-	U
332	6	26.57	2	10	-	U
333	6	26.57	2	15	-	U
334	6	26.57	2	20	-	U
335	6	26.57	2	25	-	U
336	6	26.57	2	30	-	U
337	6	26.57	2	35	-	U
338	6	26.57	2	40	-	U
339	6	26.57	2	45	-	U
340	6	26.57	5	5	-	U
341	6	26.57	5	10	-	U
342	6	26.57	5	15	-	U
343	6	26.57	5	20	-	U
344	6	26.57	5	25	-	U
345	6	26.57	5	30	-	U
346	6	26.57	5	35	-	U
347	6	26.57	5	40	-	U
348	6	26.57	5	45	-	U
349	6	26.57	10	5	-	U
350	6	26.57	10	10	-	U
351	6	26.57	10	15	-	U
352	6	26.57	10	20	-	U

Table A1. *Cont.*

Case No.	Slope Height/m	Slope Angle/°	Cohesion/kPa	Friction Angle/°	FOS	Labels
353	6	26.57	10	25	-	U
354	6	26.57	10	30	-	U
355	6	26.57	10	35	1.05	M
356	6	26.57	10	40	1.11	M
357	6	26.57	10	45	1.2	M
358	6	26.57	15	5	-	U
359	6	26.57	15	10	-	U
360	6	26.57	15	15	1.05	M
361	6	26.57	15	20	1.13	M
362	6	26.57	15	25	1.2	M
363	6	26.57	15	30	1.29	S
364	6	26.57	15	35	1.36	S
365	6	26.57	15	40	1.46	S
366	6	26.57	15	45	1.54	S
367	6	26.57	20	5	-	U
368	6	26.57	20	10	1.21	S
369	6	26.57	20	15	1.32	S
370	6	26.57	20	20	1.4	S
371	6	26.57	20	25	1.49	S
372	6	26.57	20	30	1.57	S
373	6	26.57	20	35	1.66	S
374	6	26.57	20	40	1.75	S
375	6	26.57	20	45	1.86	S
376	6	26.57	25	5	1.18	M
377	6	26.57	25	10	1.43	S
378	6	26.57	25	15	1.58	S
379	6	26.57	25	20	1.67	S
380	6	26.57	25	25	1.76	S
381	6	26.57	25	30	1.85	S
382	6	26.57	25	35	1.94	S
383	6	26.57	25	40	2.05	S
384	6	26.57	25	45	2.17	S
385	6	26.57	30	5	1.36	S
386	6	26.57	30	10	1.64	S
387	6	26.57	30	15	1.81	S
388	6	26.57	30	20	1.87	S
389	6	26.57	30	25	2.01	S
390	6	26.57	30	30	2.13	S
391	6	26.57	30	35	2.23	S
392	6	26.57	30	40	2.34	S

Table A1. *Cont.*

Case No.	Slope Height/m	Slope Angle/°	Cohesion/kPa	Friction Angle/°	FOS	Labels
393	6	26.57	30	45	2.46	S
394	6	26.57	35	5	1.51	S
395	6	26.57	35	10	1.81	S
396	6	26.57	35	15	2.03	S
397	6	26.57	35	20	2.2	S
398	6	26.57	35	25	2.27	S
399	6	26.57	35	30	2.41	S
400	6	26.57	35	35	2.5	S
401	6	26.57	35	40	2.62	S
402	6	26.57	35	45	2.74	S
403	6	26.57	40	5	1.73	S
404	6	26.57	40	10	1.99	S
405	6	26.57	40	15	2.24	S
406	6	26.57	40	20	2.45	S
407	6	26.57	40	25	2.55	S
408	6	26.57	40	30	2.68	S
409	6	26.57	40	35	2.77	S
410	6	26.57	40	40	2.9	S
411	6	26.57	40	45	3.02	S
412	6	26.57	45	5	1.88	S
413	6	26.57	45	10	2.18	S
414	6	26.57	45	15	2.45	S
415	6	26.57	45	20	2.68	S
416	6	26.57	45	25	2.84	S
417	6	26.57	45	30	2.95	S
418	6	26.57	45	35	3.06	S
419	6	26.57	45	40	3.17	S
420	6	26.57	45	45	3.31	S
421	6	26.57	50	5	2.09	S
422	6	26.57	50	10	2.36	S
423	6	26.57	50	15	2.63	S
424	6	26.57	50	20	2.86	S
425	6	26.57	50	25	3.08	S
426	6	26.57	50	30	3.15	S
427	6	26.57	50	35	3.27	S
428	6	26.57	50	40	3.45	S
429	6	26.57	50	45	3.58	S
430	6	26.57	2	0	-	U
431	6	26.57	5	0	-	U
432	6	26.57	10	0	-	U

Table A1. *Cont.*

Case No.	Slope Height/m	Slope Angle/°	Cohesion/kPa	Friction Angle/°	FOS	Labels
433	6	26.57	15	0	-	U
434	6	26.57	20	0	-	U
435	6	26.57	25	0	-	U
436	6	26.57	30	0	1.08	M
437	6	26.57	35	0	1.27	S
438	6	26.57	40	0	1.44	S
439	6	26.57	45	0	1.6	S
440	6	26.57	50	0	1.81	S
441	6	45	2	5	-	U
442	6	45	2	10	-	U
443	6	45	2	15	-	U
444	6	45	2	20	-	U
445	6	45	2	25	-	U
446	6	45	2	30	-	U
447	6	45	2	35	-	U
448	6	45	2	40	1	M
449	6	45	2	45	1.15	M
450	6	45	5	5	-	U
451	6	45	5	10	-	U
452	6	45	5	15	-	U
453	6	45	5	20	-	U
454	6	45	5	25	-	U
455	6	45	5	30	1.1	M
456	6	45	5	35	1.25	S
457	6	45	5	40	1.39	S
458	6	45	5	45	1.57	S
459	6	45	10	5	-	U
460	6	45	10	10	-	U
461	6	45	10	15	1.02	M
462	6	45	10	20	1.17	M
463	6	45	10	25	1.32	S
464	6	45	10	30	1.46	S
465	6	45	10	35	1.63	S
466	6	45	10	40	1.82	S
467	6	45	10	45	2.02	S
468	6	45	15	5	-	U
469	6	45	15	10	1.15	M
470	6	45	15	15	1.32	S
471	6	45	15	20	1.47	S
472	6	45	15	25	1.63	S

Table A1. *Cont.*

Case No.	Slope Height/m	Slope Angle/°	Cohesion/kPa	Friction Angle/°	FOS	Labels
473	6	45	15	30	1.8	S
474	6	45	15	35	1.98	S
475	6	45	15	40	2.17	S
476	6	45	15	45	2.39	S
477	6	45	20	5	1.22	S
478	6	45	20	10	1.42	S
479	6	45	20	15	1.59	S
480	6	45	20	20	1.79	S
481	6	45	20	25	1.93	S
482	6	45	20	30	2.1	S
483	6	45	20	35	2.29	S
484	6	45	20	40	2.51	S
485	6	45	20	45	2.73	S
486	6	45	25	5	1.43	S
487	6	45	25	10	1.68	S
488	6	45	25	15	1.87	S
489	6	45	25	20	2.05	S
490	6	45	25	25	2.23	S
491	6	45	25	30	2.41	S
492	6	45	25	35	2.6	S
493	6	45	25	40	2.81	S
494	6	45	25	45	3.06	S
495	6	45	30	5	1.53	S
496	6	45	30	10	1.94	S
497	6	45	30	15	2.13	S
498	6	45	30	20	2.32	S
499	6	45	30	25	2.52	S
500	6	45	30	30	2.7	S
501	6	45	30	35	2.91	S
502	6	45	30	40	3.12	S
503	6	45	30	45	3.38	S
504	6	45	35	5	1.97	S
505	6	45	35	10	2.19	S
506	6	45	35	15	2.38	S
507	6	45	35	20	2.6	S
508	6	45	35	25	2.79	S
509	6	45	35	30	3.01	S
510	6	45	35	35	3.2	S
511	6	45	35	40	3.42	S
512	6	45	35	45	3.67	S

Table A1. *Cont.*

Case No.	Slope Height/m	Slope Angle/°	Cohesion/kPa	Friction Angle/°	FOS	Labels
513	6	45	40	5	2.22	S
514	6	45	40	10	2.44	S
515	6	45	40	15	2.65	S
516	6	45	40	20	2.85	S
517	6	45	40	25	3.08	S
518	6	45	40	30	3.3	S
519	6	45	40	35	3.55	S
520	6	45	40	40	3.7	S
521	6	45	40	45	3.98	S
522	6	45	45	5	2.46	S
523	6	45	45	10	2.71	S
524	6	45	45	15	2.9	S
525	6	45	45	20	3.12	S
526	6	45	45	25	3.32	S
527	6	45	45	30	3.55	S
528	6	45	45	35	3.81	S
529	6	45	45	40	4.04	S
530	6	45	45	45	4.27	S
531	6	45	50	5	2.71	S
532	6	45	50	10	2.95	S
533	6	45	50	15	3.15	S
534	6	45	50	20	3.37	S
535	6	45	50	25	3.58	S
536	6	45	50	30	3.8	S
537	6	45	50	35	4.07	S
538	6	45	50	40	4.33	S
539	6	45	50	45	4.57	S
540	6	45	2	0	-	U
541	6	45	5	0	-	U
542	6	45	10	0	-	U
543	6	45	15	0	-	U
544	6	45	20	0	1	M
545	6	45	25	0	1.2	M
546	6	45	30	0	1.46	S
547	6	45	35	0	1.61	S
548	6	45	40	0	1.95	S
549	6	45	45	0	2.19	S
550	6	45	50	0	2.37	S
551	6	63.43	2	5	-	U
552	6	63.43	2	10	-	U

Table A1. *Cont.*

Case No.	Slope Height/m	Slope Angle/°	Cohesion/kPa	Friction Angle/°	FOS	Labels
553	6	63.43	2	15	-	U
554	6	63.43	2	20	-	U
555	6	63.43	2	25	-	U
556	6	63.43	2	30	-	U
557	6	63.43	2	35	-	U
558	6	63.43	2	40	-	U
559	6	63.43	2	45	-	U
560	6	63.43	5	5	-	U
561	6	63.43	5	10	-	U
562	6	63.43	5	15	-	U
563	6	63.43	5	20	-	U
564	6	63.43	5	25	-	U
565	6	63.43	5	30	-	U
566	6	63.43	5	35	-	U
567	6	63.43	5	40	-	U
568	6	63.43	5	45	1.01	M
569	6	63.43	10	5	-	U
570	6	63.43	10	10	-	U
571	6	63.43	10	15	-	U
572	6	63.43	10	20	-	U
573	6	63.43	10	25	-	U
574	6	63.43	10	30	1.07	M
575	6	63.43	10	35	1.16	M
576	6	63.43	10	40	1.31	S
577	6	63.43	10	45	1.39	S
578	6	63.43	15	5	-	U
579	6	63.43	15	10	-	U
580	6	63.43	15	15	1.04	M
581	6	63.43	15	20	1.14	M
582	6	63.43	15	25	1.25	S
583	6	63.43	15	30	1.35	S
584	6	63.43	15	35	1.46	S
585	6	63.43	15	40	1.59	S
586	6	63.43	15	45	1.75	S
587	6	63.43	20	5	1.03	M
588	6	63.43	20	10	1.16	M
589	6	63.43	20	15	1.29	S
590	6	63.43	20	20	1.41	S
591	6	63.43	20	25	1.52	S
592	6	63.43	20	30	1.63	S

Table A1. *Cont.*

Case No.	Slope Height/m	Slope Angle/°	Cohesion/kPa	Friction Angle/°	FOS	Labels
593	6	63.43	20	35	1.74	S
594	6	63.43	20	40	1.87	S
595	6	63.43	20	45	2.02	S
596	6	63.43	25	5	1.26	S
597	6	63.43	25	10	1.39	S
598	6	63.43	25	15	1.53	S
599	6	63.43	25	20	1.65	S
600	6	63.43	25	25	1.77	S
601	6	63.43	25	30	1.9	S
602	6	63.43	25	35	2.02	S
603	6	63.43	25	40	2.15	S
604	6	63.43	25	45	2.28	S
605	6	63.43	30	5	1.48	S
606	6	63.43	30	10	1.63	S
607	6	63.43	30	15	1.75	S
608	6	63.43	30	20	1.88	S
609	6	63.43	30	25	2.01	S
610	6	63.43	30	30	2.15	S
611	6	63.43	30	35	2.29	S
612	6	63.43	30	40	2.42	S
613	6	63.43	30	45	2.55	S
614	6	63.43	35	5	1.71	S
615	6	63.43	35	10	1.84	S
616	6	63.43	35	15	1.99	S
617	6	63.43	35	20	2.12	S
618	6	63.43	35	25	2.25	S
619	6	63.43	35	30	2.39	S
620	6	63.43	35	35	2.54	S
621	6	63.43	35	40	2.69	S
622	6	63.43	35	45	2.84	S
623	6	63.43	40	5	1.92	S
624	6	63.43	40	10	2.08	S
625	6	63.43	40	15	2.21	S
626	6	63.43	40	20	2.35	S
627	6	63.43	40	25	2.49	S
628	6	63.43	40	30	2.63	S
629	6	63.43	40	35	2.78	S
630	6	63.43	40	40	2.94	S
631	6	63.43	40	45	3.13	S
632	6	63.43	45	5	2.14	S

Table A1. *Cont.*

Case No.	Slope Height/m	Slope Angle/°	Cohesion/kPa	Friction Angle/°	FOS	Labels
633	6	63.43	45	10	2.29	S
634	6	63.43	45	15	2.43	S
635	6	63.43	45	20	2.57	S
636	6	63.43	45	25	2.71	S
637	6	63.43	45	30	2.86	S
638	6	63.43	45	35	3.02	S
639	6	63.43	45	40	3.18	S
640	6	63.43	45	45	3.37	S
641	6	63.43	50	5	2.36	S
642	6	63.43	50	10	2.53	S
643	6	63.43	50	15	2.67	S
644	6	63.43	50	20	2.81	S
645	6	63.43	50	25	2.95	S
646	6	63.43	50	30	3.09	S
647	6	63.43	50	35	3.25	S
648	6	63.43	50	40	3.44	S
649	6	63.43	50	45	3.61	S
650	6	63.43	2	0	-	U
651	6	63.43	5	0	-	U
652	6	63.43	10	0	-	U
653	6	63.43	15	0	-	U
654	6	63.43	20	0	-	U
655	6	63.43	25	0	1.07	M
656	6	63.43	30	0	1.33	S
657	6	63.43	35	0	1.55	S
658	6	63.43	40	0	1.76	S
659	6	63.43	45	0	1.97	S
660	6	63.43	50	0	2.2	S
661	12	45	2	5	-	U
662	12	45	2	10	-	U
663	12	45	2	15	-	U
664	12	45	2	20	-	U
665	12	45	2	25	-	U
666	12	45	2	30	-	U
667	12	45	2	35	-	U
668	12	45	2	40	-	U
669	12	45	2	45	1	M
670	12	45	5	5	-	U
671	12	45	5	10	-	U
672	12	45	5	15	-	U

Table A1. *Cont.*

Case No.	Slope Height/m	Slope Angle/°	Cohesion/kPa	Friction Angle/°	FOS	Labels
673	12	45	5	20	-	U
674	12	45	5	25	-	U
675	12	45	5	30	-	U
676	12	45	5	35	-	U
677	12	45	5	40	1.04	M
678	12	45	5	45	1.19	M
679	12	45	10	5	-	U
680	12	45	10	10	-	U
681	12	45	10	15	-	U
682	12	45	10	20	-	U
683	12	45	10	25	-	U
684	12	45	10	30	1.06	M
685	12	45	10	35	1.2	M
686	12	45	10	40	1.33	S
687	12	45	10	45	1.47	S
688	12	45	15	5	-	U
689	12	45	15	10	-	U
690	12	45	15	15	-	U
691	12	45	15	20	-	U
692	12	45	15	25	1.11	M
693	12	45	15	30	1.26	S
694	12	45	15	35	1.4	S
695	12	45	15	40	1.55	S
696	12	45	15	45	1.71	S
697	12	45	20	5	-	U
698	12	45	20	10	-	U
699	12	45	20	15	1	M
700	12	45	20	20	1.12	M
701	12	45	20	25	1.29	S
702	12	45	20	30	1.42	S
703	12	45	20	35	1.57	S
704	12	45	20	40	1.76	S
705	12	45	20	45	1.96	S
706	12	45	25	5	-	U
707	12	45	25	10	-	U
708	12	45	25	15	1.13	M
709	12	45	25	20	1.26	S
710	12	45	25	25	1.44	S
711	12	45	25	30	1.6	S
712	12	45	25	35	1.75	S

Table A1. *Cont.*

Case No.	Slope Height/m	Slope Angle/°	Cohesion/kPa	Friction Angle/°	FOS	Labels
713	12	45	25	40	1.93	S
714	12	45	25	45	2.14	S
715	12	45	30	5	-	U
716	12	45	30	10	1.07	M
717	12	45	30	15	1.22	S
718	12	45	30	20	1.43	S
719	12	45	30	25	1.55	S
720	12	45	30	30	1.74	S
721	12	45	30	35	1.93	S
722	12	45	30	40	2.11	S
723	12	45	30	45	2.3	S
724	12	45	35	5	1.01	M
725	12	45	35	10	1.19	M
726	12	45	35	15	1.37	S
727	12	45	35	20	1.53	S
728	12	45	35	25	1.67	S
729	12	45	35	30	1.89	S
730	12	45	35	35	2.07	S
731	12	45	35	40	2.27	S
732	12	45	35	45	2.47	S
733	12	45	40	5	1.1	M
734	12	45	40	10	1.29	S
735	12	45	40	15	1.45	S
736	12	45	40	20	1.64	S
737	12	45	40	25	1.86	S
738	12	45	40	30	1.97	S
739	12	45	40	35	2.22	S
740	12	45	40	40	2.44	S
741	12	45	40	45	2.65	S
742	12	45	45	5	1.23	S
743	12	45	45	10	1.42	S
744	12	45	45	15	1.59	S
745	12	45	45	20	1.75	S
746	12	45	45	25	1.97	S
747	12	45	45	30	2.11	S
748	12	45	45	35	2.35	S
749	12	45	45	40	2.57	S
750	12	45	45	45	2.79	S
751	12	45	50	5	1.34	S
752	12	45	50	10	1.53	S

Table A1. *Cont.*

Case No.	Slope Height/m	Slope Angle/°	Cohesion/kPa	Friction Angle/°	FOS	Labels
753	12	45	50	15	1.72	S
754	12	45	50	20	1.89	S
755	12	45	50	25	2.07	S
756	12	45	50	30	2.31	S
757	12	45	50	35	2.52	S
758	12	45	50	40	2.73	S
759	12	45	50	45	2.96	S
760	12	45	2	0	-	U
761	12	45	5	0	-	U
762	12	45	10	0	-	U
763	12	45	15	0	-	U
764	12	45	20	0	-	U
765	12	45	25	0	-	U
766	12	45	30	0	-	U
767	12	45	35	0	-	U
768	12	45	40	0	-	U
769	12	45	45	0	1.04	M
770	12	45	50	0	1.15	M
771	12	63.43	2	5	-	U
772	12	63.43	2	10	-	U
773	12	63.43	2	15	-	U
774	12	63.43	2	20	-	U
775	12	63.43	2	25	-	U
776	12	63.43	2	30	-	U
777	12	63.43	2	35	-	U
778	12	63.43	2	40	-	U
779	12	63.43	2	45	-	U
780	12	63.43	5	5	-	U
781	12	63.43	5	10	-	U
782	12	63.43	5	15	-	U
783	12	63.43	5	20	-	U
784	12	63.43	5	25	-	U
785	12	63.43	5	30	-	U
786	12	63.43	5	35	-	U
787	12	63.43	5	40	-	U
788	12	63.43	5	45	-	U
789	12	63.43	10	5	-	U
790	12	63.43	10	10	-	U
791	12	63.43	10	15	-	U
792	12	63.43	10	20	-	U

Table A1. *Cont.*

Case No.	Slope Height/m	Slope Angle/°	Cohesion/kPa	Friction Angle/°	FOS	Labels
793	12	63.43	10	25	-	U
794	12	63.43	10	30	-	U
795	12	63.43	10	35	-	U
796	12	63.43	10	40	-	U
797	12	63.43	10	45	1.02	M
798	12	63.43	15	5	-	U
799	12	63.43	15	10	-	U
800	12	63.43	15	15	-	U
801	12	63.43	15	20	-	U
802	12	63.43	15	25	-	U
803	12	63.43	15	30	-	U
804	12	63.43	15	35	-	U
805	12	63.43	15	40	1.04	M
806	12	63.43	15	45	1.14	M
807	12	63.43	20	5	-	U
808	12	63.43	20	10	-	U
809	12	63.43	20	15	-	U
810	12	63.43	20	20	-	U
811	12	63.43	20	25	-	U
812	12	63.43	20	30	1.04	M
813	12	63.43	20	35	1.14	M
814	12	63.43	20	40	1.21	S
815	12	63.43	20	45	1.31	S
816	12	63.43	25	5	-	U
817	12	63.43	25	10	-	U
818	12	63.43	25	15	-	U
819	12	63.43	25	20	-	U
820	12	63.43	25	25	1.09	M
821	12	63.43	25	30	1.19	M
822	12	63.43	25	35	1.3	S
823	12	63.43	25	40	1.39	S
824	12	63.43	25	45	1.48	S
825	12	63.43	30	5	-	U
826	12	63.43	30	10	-	U
827	12	63.43	30	15	1.01	M
828	12	63.43	30	20	1.13	M
829	12	63.43	30	25	1.23	S
830	12	63.43	30	30	1.31	S
831	12	63.43	30	35	1.42	S
832	12	63.43	30	40	1.54	S

Table A1. *Cont.*

Case No.	Slope Height/m	Slope Angle/°	Cohesion/kPa	Friction Angle/°	FOS	Labels
833	12	63.43	30	45	1.66	S
834	12	63.43	35	5	-	U
835	12	63.43	35	10	1.03	M
836	12	63.43	35	15	1.14	M
837	12	63.43	35	20	1.27	S
838	12	63.43	35	25	1.35	S
839	12	63.43	35	30	1.46	S
840	12	63.43	35	35	1.56	S
841	12	63.43	35	40	1.62	S
842	12	63.43	35	45	1.81	S
843	12	63.43	40	5	1.01	M
844	12	63.43	40	10	1.13	M
845	12	63.43	40	15	1.29	S
846	12	63.43	40	20	1.24	S
847	12	63.43	40	25	1.49	S
848	12	63.43	40	30	1.58	S
849	12	63.43	40	35	1.7	S
850	12	63.43	40	40	1.81	S
851	12	63.43	40	45	1.97	S
852	12	63.43	45	5	1.13	M
853	12	63.43	45	10	1.25	S
854	12	63.43	45	15	1.4	S
855	12	63.43	45	20	1.51	S
856	12	63.43	45	25	1.64	S
857	12	63.43	45	30	1.73	S
858	12	63.43	45	35	1.83	S
859	12	63.43	45	40	1.96	S
860	12	63.43	45	45	2.07	S
861	12	63.43	50	5	1.21	S
862	12	63.43	50	10	1.31	S
863	12	63.43	50	15	1.49	S
864	12	63.43	50	20	1.64	S
865	12	63.43	50	25	1.7	S
866	12	63.43	50	30	1.83	S
867	12	63.43	50	35	1.97	S
868	12	63.43	50	40	2.06	S
869	12	63.43	50	45	2.24	S
870	12	63.43	2	0	-	U
871	12	63.43	5	0	-	U
872	12	63.43	10	0	-	U

Table A1. *Cont.*

Case No.	Slope Height/m	Slope Angle/°	Cohesion/kPa	Friction Angle/°	FOS	Labels
873	12	63.43	15	0	-	U
874	12	63.43	20	0	-	U
875	12	63.43	25	0	-	U
876	12	63.43	30	0	-	U
877	12	63.43	35	0	-	U
878	12	63.43	40	0	-	U
879	12	63.43	45	0	-	U
880	12	63.43	50	0	1.03	M

References

1. Massey, C.; Della Pasqua, F.; Holden, C.; Kaiser, A.; Richards, L.; Wartman, J.; McSaveney, M.J.; Archibald, G.; Yetton, M.; Janku, L. Rock slope response to strong earthquake shaking. *Landslides* **2017**, *14*, 249–268. [CrossRef]
2. Li, Q.; Wang, Y.M.; Zhang, K.B.; Yu, H.; Tao, Z.Y. Field investigation and numerical study of a siltstone slope instability induced by excavation and rainfall. *Landslides* **2020**, *17*, 1485–1499. [CrossRef]
3. Nagatani, K.; Abe, M.; Osuka, K.; Chun, P.-j.; Okatani, T.; Nishio, M.; Chikushi, S.; Matsubara, T.; Ikemoto, Y.; Asama, H. Innovative technologies for infrastructure construction and maintenance through collaborative robots based on an open design approach. *Adv. Robot.* **2021**, *2021*, 715–722. [CrossRef]
4. Das, S.K.; Biswal, R.K.; Sivakugan, N.; Das, B. Classification of slopes and prediction of factor of safety using differential evolution neural networks. *Environ. Earth Sci.* **2011**, *64*, 201–210. [CrossRef]
5. Sloan, S.W. Geotechnical stability analysis. *Geotechnique* **2013**, *63*, 531–572. [CrossRef]
6. Cheng, Y.M.; Lansivaara, T.; Wei, W.B. Two-dimensional slope stability analysis by limit equilibrium and strength reduction methods. *Comput. Geotech.* **2007**, *34*, 137–150. [CrossRef]
7. Reale, C.; Xue, J.; Gavin, K. System reliability of slopes using multimodal optimisation. *Geotechnique* **2016**, *66*, 413–423. [CrossRef]
8. Tschuchnigg, F.; Schweiger, H.F.; Sloan, S.W.; Lyamin, A.V.; Raissakis, I. Comparison of finite-element limit analysis and strength reduction techniques. *Geotechnique* **2015**, *65*, 249–257. [CrossRef]
9. Song, D.; Chen, Z.; Chao, H.; Ke, Y.; Nie, W. Numerical study on seismic response of a rock slope with discontinuities based on the time-frequency joint analysis method. *Soil Dyn. Earthq. Eng.* **2020**, *133*, 106112. [CrossRef]
10. Sakellariou, M.G.; Ferentinou, M.D. A study of slope stability prediction using neural networks. *Geotech. Geol. Eng.* **2005**, *23*, 419–445. [CrossRef]
11. Samui, P. Slope stability analysis: A support vector machine approach. *Environ. Geol.* **2008**, *56*, 255–267. [CrossRef]
12. Zhou, J.; Li, E.; Yang, S.; Wang, M.; Shi, X.; Yao, S.; Mitri, H.S. Slope stability prediction for circular mode failure using gradient boosting machine approach based on an updated database of case histories. *Saf. Sci.* **2019**, *118*, 505–518. [CrossRef]
13. Mahmoodzadeh, A.; Mohammadi, M.; Farid Hama Ali, H.; Hashim Ibrahim, H.; Nariman Abdulhamid, S.; Nejati, H.R. Prediction of safety factors for slope stability: Comparison of machine learning techniques. *Nat. Hazards* **2022**, *111*, 1771–1799. [CrossRef]
14. Shi, N.; Xu, J.; Wurster, S.W.; Guo, H.; Woodring, J.; Van Roekel, L.P.; Shen, H.W. GNN-Surrogate: A Hierarchical and Adaptive Graph Neural Network for Parameter Space Exploration of Unstructured-Mesh Ocean Simulations. *IEEE Trans. Vis. Comput. Graph.* **2022**, *28*, 2301–2313. [CrossRef] [PubMed]
15. Jain, A.K.; Mao, J.; Mohiuddin, K.M. Artificial neural networks: A tutorial. *Computer* **1996**, *29*, 31–44. [CrossRef]
16. Dreiseitl, S.; Ohno-Machado, L. Logistic regression and artificial neural network classification models: A methodology review. *J. Biomed. Inform.* **2002**, *35*, 352–359. [CrossRef]
17. Georgevici, A.I.; Terblanche, M. Neural networks and deep learning: A brief introduction. *Intensive Care Med.* **2019**, *45*, 712–714. [CrossRef]
18. Dahiya, N.; Saini, B.; Chalak, H.D. Deep neural network-based storey drift modelling of precast concrete structures using RStudio. *J. Soft Comput. Civ. Eng.* **2021**, *5*, 88–100. [CrossRef]
19. Yamane, T.; Chun, P.-J. Crack detection from a concrete surface image based on semantic segmentation using deep learning. *J. Adv. Concr. Technol.* **2020**, *18*, 493–504. [CrossRef]
20. Chun, P.-j.; Yamane, T.; Tsuzuki, Y. Automatic detection of cracks in asphalt pavement using deep learning to overcome weaknesses in images and gis visualization. *Appl. Sci.* **2021**, *11*, 892. [CrossRef]
21. Chun, P.-j.; Yamane, T.; Maemura, Y. A deep learning-based image captioning method to automatically generate comprehensive explanations of bridge damage. *Comput. Civ. Infrastruct. Eng.* **2022**, *37*, 1387–1401. [CrossRef]
22. Yamane, T.; Chun, P.-j.; Dang, J.; Honda, R. Recording of bridge damage areas by 3D integration of multiple images and reduction of the variability in detected results. *Comput. Civ. Infrastruct. Eng.* **2023**, 1–17. [CrossRef]

23. Xu, J.J.; Zhang, H.; Tang, C.S.; Cheng, Q.; Liu, B.; Shi, B. Automatic soil desiccation crack recognition using deep learning. *Geotechnique* **2022**, *72*, 337–349. [CrossRef]
24. Lozano-Diez, A.; Zazo, R.; Toledano, D.T.; Gonzalez-Rodriguez, J. An analysis of the influence of deep neural network (DNN) topology in bottleneck feature based language recognition. *PLoS ONE* **2017**, *12*, e0182580. [CrossRef]
25. Xu, Y.; Du, J.; Dai, L.R.; Lee, C.H. A regression approach to speech enhancement based on deep neural networks. *IEEE/ACM Trans. Audio Speech Lang. Process.* **2015**, *23*, 7–19. [CrossRef]
26. Liu, S.Y.; Shao, L.T.; Li, H.J. Slope stability analysis using the limit equilibrium method and two finite element methods. *Comput. Geotech.* **2015**, *63*, 291–298. [CrossRef]